2017 IEEE International Conference on Robotics and Automation (ICRA)
Singapore, May 29 - June 3, 2017

Bayesian Estimation based Real-Time Fire-Heading in Smoke-Filled Indoor Environments Using Thermal Imagery

Jong-Hwan Kim, Yoonchang Sung and Brian Y Lattimer, *Member, IEEE*

***Abstract*— This paper presents a fire heading estimation for solving the autonomous navigation problem of a firefighting robot in smoke-filled indoor fire environment. In smoke-filled fire environments, firefighters and firefighting robots experience difficulty maintaining direction while finding the fire source. To solve this, the statistical texture features in thermal images were analyzed and fused by using Bayesian estimation to compute the vertical and horizontal fire heading. For its validation, a large-scaled test-bed was built with a hallway and two rooms, with one of the rooms having a real size fire generating dense and dark smoke. The proposed method probabilistically computed the fire-heading toward the entrance of the hallway then guided the robot to the room with the actual fire, all while navigating in a smoke-filled situation. The experimental results have demonstrated the effectiveness of this method in indoor fire environments.**

I. Introduction

Intelligent firefighting robots are actively being researched to reduce firefighter injuries and deaths as well as increase their effectiveness on performing tasks [1-6]. One task is locating a fire inside of a structure outside the robot field of view (FOV). For this task, fire, smoke, and their thermal reflections can be clues to determine a heading that will eventually lead the robot to the fire so that it can suppress it. However, research for accurately estimating the fire heading in smoke-filled indoor fire environments has been incomplete.

Fire heading estimation in smoke-filled indoor fire environments is challenging because the sensors that had been generally used for autonomous navigation of robots such as CCD camera, LIDAR, and sonar, did not function due to dense smoke and high temperature. In addition, because fire environments can change rapidly and unexpectedly, information in the robot FOV cannot be accurate to detect and identify fire and smoke that are clues to find the fire source. In conventional fire (and/or smoke) detection systems [7-10], temperature, ionization and ultraviolet light were mainly used to point out the presence of a fire and/or smoke inside the structure, but they cannot provide sufficient data for the location of fire and/or smoke in smoke-filled environments. Recently long-wavelength thermal cameras, similar to the handheld thermal infrared cameras (TIC) that are typically used to assist firefighting tasks within smoke-filled environments [11-14], were used in this research. Due to the fact that TICs absorb infrared radiation in the long wavelength IR (7-14 microns), they are capable of imaging surfaces even in dense smoke and zero visibility environments [2, 15]. In addition, TIC can provide clear information under local or global darkness, e.g. shadows or darkness caused by damaged lighting indoors. The cameras will detect hot objects as well as thermal reflections off of surfaces. Thus, a TIC was used for the fire heading estimation of the intelligent firefighting robot.

Fig. 1. The shipboard autonomous firefighting robot (SAFFiR) [16].

A temperature based fire heading estimation was studied in [17] by analyzing temperature distribution surroundings. This study used thermal images to find the highest temperature area which is related to the high probability of fire presence. However, because this study considered only a single feature i.e. temperature, objects collected that have high temperature e.g. hot objects or thermal reflections on walls were sparsely determined as the fire heading. This resulted in navigation failure of the firefighting robot. In order to overcome this problem, another study was implemented to probabilistically classify fire, smoke, their thermal reflections and hot objects using Bayesian theory [18]. This study extracted four statistical texture features from objects in thermal images and probabilistically classified multiple classes in real-time. However, this study did not provide an

Jong-Hwan Kim is with Korea Military Academy, Seoul, South Korea (82+02-2197-2959, e-mail: jonghwan7028@gmail.com)
Yoonchang Sung is with Virginia Tech, Blacksburg, VA 24060 USA. (e-mail: syc7446@gmail.com).
Brian Lattimer is with Virginia Tech, Blacksburg, VA 24060 USA. (e-mail: blattimer@ jensenhughes.com).

exact direction for the firefighting robot to move toward the fire. In order to apply into humanoid robots and/or UAVs for firefighting tasks, an accurate vertical and horizontal heading directions needed to be researched.

This paper presents a real-time fire heading estimation in smoke-filled indoor fire environments. The Bayesian estimation was applied to estimate the heading which indicates a horizontal and vertical direction for navigating toward the fire outside the FOV. Five statistical texture features in thermal images were extracted to accurately compute the highest probability for the heading. The proposed method was developed for SAFFiR (Shipboard Autonomous Firefighting Robot), an autonomous humanoid firefighting robot in Fig. 1. For its validation, large-scale fire tests were conducted to create actual fire environments having various ranges of temperature and smoke conditions.

II. System Architecture

A vertical and horizontal fire heading is probabilistically estimated in real-time to provide SAFFiR with information to navigate toward a fire that is outside the robot FOV. As shown in Fig. 2, system architecture consists of five stages; thermal image acquisition, object detection and classification, statistical texture feature extraction, recursive Bayesian estimation, and fire heading display. Both thermal image acquisition and object detection & classification stages were researched previously [16], and the rest of stages were further studied to estimate the exact direction toward fire source based on the previous results. In the stage of thermal image acquisition, a FLIR A35 long wavelength infrared (7-14 micron) camera is mounted on the SAFFiR head and used to provide 14-bit gray-level thermal images with intensity range between -16384 for -40 °C and -1 for 550 °C as well as a 320×256-pixel focal plane array with 60 Hz frame rates. Next, during object detection and classification, objects from images that have the highest likelihood to be fire, smoke, or their reflections are extracted from the scene by adaptive background subtraction and morphological filtering, and probabilistically classified to fire, smoke, their thermal reflections and other objects [16]. In the stage of statistical texture feature extraction, five statistical texture features are extracted from the objects which are then classified as smoke and fire. Then, in the stage of recursive Bayesian estimation (RBE), Bayes theory is applied by fusing the five statistical texture features into $n \times n$ grids on the objects. RBE is used to estimate the highest probability of fire existence that is linked to the vertical and horizontal fire heading. Lastly, the classification results and the fire heading (a red cross) are displayed simultaneously on the screen.

Fig. 3. Visual image (left) and original thermal image (right) in the robot FOV at the entrance of the hallway in the experiments.

A. Thermal image acquisition

A main characteristic of fire and smoke classification is that they are higher in temperature than the background. Since temperature is associated to intensity in thermal images, fire and smoke regions show brighter than the background. Thus, intensity is a primary factor when subtracting the foreground from the background.

B. Object detection and classification

The intensity histogram from a thermal image changes consistently as the surrounding environment of the fire changes. Manual thresholding and model-based techniques are less efficient because they require frequent update process to find the optimum parameters [19, 20]. A clustering-based image technique called Otsu's method [21] is used to discriminate the two classes, foreground (objects) and background, resulting in fast computation during real-time implementation. It can also deal with rapidly changing environments by analyzing the intensity histogram and updating an optimum threshold at each scene. This image auto-thresholding computes the optimum threshold that minimizes the weighted sum of variances of both classes to separate. A 14-bit gray-level histogram from thermal images is normalized and a probability distribution can be described in Eq. (1)

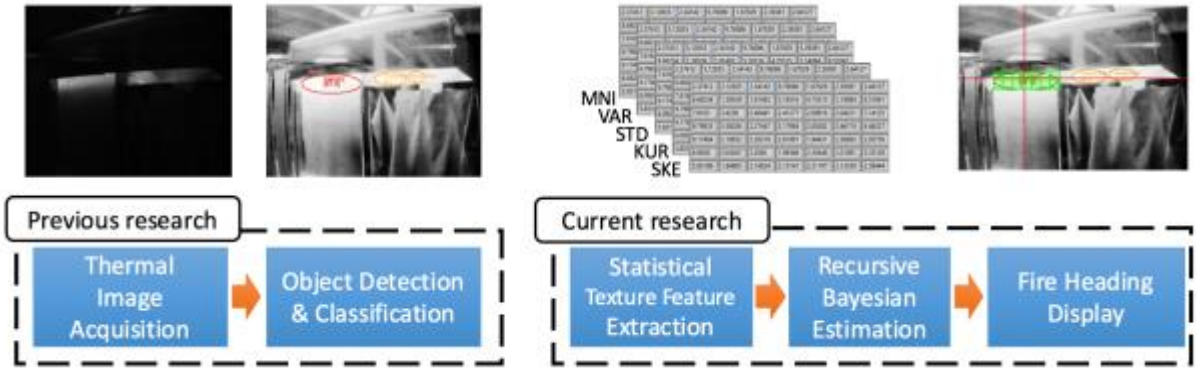

Fig. 2. System architecture of autonomous fire heading estimation.

$$p_i = \frac{n_i}{N}, \sum_{i=-16384}^{-1} p_i \quad (1)$$

where n_i is the number of pixels at histogram level i and N is the total number of pixels. For the separation threshold level k, the occurrence probabilities of both foreground and background can be calculated as follows,

$$w_F(k) = \sum_{i=k+1}^{-1} p_i, \quad w_B(k) = \sum_{i=-16384}^{k} p_i \quad (2)$$

and the mean probabilities of both foreground and background can be calculated by Eq. (3).

$$\mu_F(k) = \sum_{i=k+1}^{-1} \frac{ip_i}{w_F}, \quad \mu_B(k) = \sum_{i=-16384}^{k} \frac{ip_i}{w_B} \quad (3)$$

The between-class variance σ_{BC}^2 in the discriminant analysis can be calculated by Eq. (4) and the optimum threshold k for both classes separation can be computed by Eq. (5).

$$\sigma_{BC}^2(k) = w_F(k)w_B(k)\left[\mu_F(k) - \mu_B(k)\right]^2 \quad (4)$$

$$T_{opt} = \underset{-16384 \le k \le -1}{\operatorname{argmax}} \sigma_{BC}^2(k) \quad (5)$$

For background subtraction, both classes are defined as a binary image with 1 being the foreground (i.e. objects) and 0 being the background based on the optimum threshold calculation. Using morphological filtering techniques, the binary images are filtered to remove small regions of interest (ROI) from the image and also holes inside objects ROI are removed. By implementing convolution both the original 14-bit image and the filtered-binary image, an image is obtained that includes the original 14-bit intensities in objects ROI as well as zeroes in the rest of the image.

The objects are categorized into five classes, fire, smoke, their reflections and other hot objects. To characterize these objects, four statistical texture features were analyzed because texture features are less influenced by rotation and motion of a robot. The first order statistical textures estimate the individual property of pixels not having any relationship between neighboring pixels. Both mean intensity (MNI) and variance (VAR) are computed using the intensity histogram of the candidate ROI in the image. The second order statistical textures represent spatial relationships between a pixel and its neighbors. Both entropy (ENT) and inverse difference moment (IDM) are calculated using the gray-level co-occurrence matrix (GLCM) [22] which accounts for adjacent pixel relationships with four directions (horizontal, vertical, left and right diagonals) by quantizing the spatial co-occurrence of neighboring pixels. The third and higher order statistic features are not studied in this research due to computational expense. MNI and VAR in the first order texture features can be written as,

$$\text{MNI}(\mu) = \frac{1}{N_P} \sum_{i,j=1}^{N_P} I_{i,j} \quad (7)$$

$$\text{VAR} = \frac{1}{N_P} \sum_{i,j=1}^{N_P} \left(I_{i,j} - \mu\right)^2 \quad (8)$$

where $I_{i,j}$ refers to the intensity of a pixel at i and j and N_P denotes the number of pixels of the object in the image. Both ENT and VAR in the second order statistic features are calculated by a normalized co-occurrence matrix, $C_{i,j}$ which can be described as,

$$C_{i,j} = \frac{P_{i,j}}{\sum_{i,j=1}^{N_G} P_{i,j}} \quad (9)$$

where $P_{i,j}$ denotes to the frequency of occurrences of the grey-level of adjacent pixels at i and j within the four directions and N_G refers to the number of the grey levels in the quantized image.

$$\text{ENT} = -\sum C_{i,j} log C_{i,j} \quad (10)$$

$$\text{IDM} = \sum \frac{C_{i,j}}{1+(i-j)^2} \quad (11)$$

Using these features $F_1, F_2, \ldots, F_q$ $(q = 4)$, Bayesian classifier was applied to calculate the probability that one class C_h corresponds to the object k by using a conditional probability, the posterior probability, ${}^k p(C_h|F_1F_2 \ldots F\_q)$ which can be written as,

$${}^k p\left(C_h \middle| F_1F_2 \ldots F_q\right) = \frac{{}^k p(C_h)\, {}^k f\left(F_1F_2 \ldots F_q \middle| C_h\right)}{\sum_{C_h} {}^k p(C_h)\, {}^k f\left(F_1F_2 \ldots F_q \middle| C_h\right)} \quad (12)$$

where ${}^k p(C_h)$ is the prior probability, meaning it represents object k probability to be C_h and can be calculated by number of samples of class C_h divided by the total number of samples. ${}^k f\left(F_1F_2 \ldots F_q|C_h\right)$ is the likelihood function,

$$f\left(F_1F_2 \ldots F_q \middle| C_h\right) = \prod_{i=1}^{q} f(F_i|C_h) \quad (13)$$

The denominator of Eq. (12) is the evidence that plays as a normalizing constant by the summation of production between the prior and likelihood at each class. With Eq. (13), the evidence and then the posterior probability of each class were computed. By applying the maximum priority decision rule in Eq. (14) and (15), the Bayesian classification predicts the class and probability of each candidate in the scene. The objects in the thermal image are highlighted by colored ellipses. The results of the class and probability of each object are displayed at the center of the ellipses. While the red represents smoke and fire, the orange shows their thermal reflections. Also, the adaptive histogram equalization [23] was implemented to improve image display and to solve a bias problem in the thermal image histogram.

(a) (b)

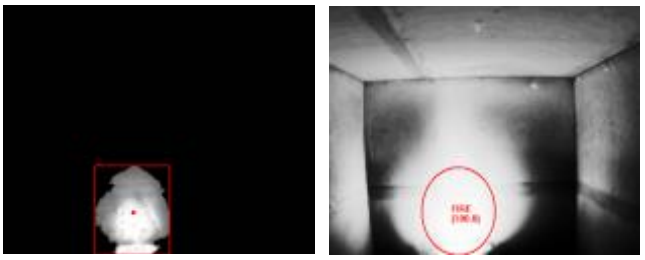

(c) (d)

Fig. 4. Results of the object detection by image processing and probabilistic classification by Bayesian classifier. (a) original visual image, (b) original thermal image, (c) background subtraction and object detection result, and (d) classification result in a room where a fire is present.

C. Statistical texture feature extraction

In order to estimate the fire heading on the thermal images, five statistical texture features are extracted from the objects classified as both fire and smoke. Because thermal reflections of fire and smoke may lead the robot toward a wrong direction, only fire and smoke objects are mainly considered as key objects. In addition, a 7×7 grid over the key objects is created and the mean intensity (MNI), variance (VAR), standard deviation (STD), kurtosis (KUR), and skewness (SKE) in the first order statistical texture features are calculated at each grid. These five features assess individual property of pixels, not characterizing any relationship between neighboring pixels and can be described as,

$$\mathrm{STD}(\sigma) = \left\{ \frac{1}{N_p} \sum_{i,j=1}^{N_p} \left(I_{i,j} - \mu\right)^2 \right\}^{\frac{1}{2}} \tag{14}$$

$$\mathrm{SKE} = \frac{1}{\sigma^3 N_p} \sum_{i,j=1}^{N_p} \left(I_{i,j} - \mu\right)^3 \tag{15}$$

$$\mathrm{KUR} = \frac{1}{\sigma^4 N_p} \sum_{i,j=1}^{N_p} \left(I_{i,j} - \mu\right)^4 \tag{16}$$

D. Recursive Bayesian estimation

Consider the firefighting robot *t* to navigate toward the fire source, the motion of which is discretely defined by, $x_{k+1}^t = f^t(x_k^t, u_k^t, w_k^t)$, where $x_k^t \in \mathcal{X}^t$ is the state of the target at time step k, which in general describes its horizontal and vertical positions in the thermal image, $u_k^t \in \mathcal{U}^t$ is the set of control inputs of the target, $w_k^t \in \mathcal{W}^t$ is the "systems noise" of the target which includes external inputs such as robot motion and smoke flow in fire environments.

In order for the fire heading estimation problem, this moving target is observed by a sensor platform *s*. The sensor platform carries an optical sensor to observe the target. The observation from the sensor platform *s*, ${}^s x_k \in \mathcal{X}^t$, is subject to observation noise v_k^s, ${}^s z_k = h^s(x_k^s, v_k^s)$. Note that the observation model included the five statistical texture features and recursively estimates the fire heading in real-time.

1) Update

The update equation calculates the posterior density $p\left(x_k^t \middle| {}^{s_{i:n_s}}\tilde{z}_{1:k}, \tilde{x}_{1:k}^s\right)$ given the corresponding state estimated $p\left(x_k^t \middle| {}^{s_{i:n_s}}\tilde{z}_{1:k-1}, \tilde{x}_{1:k}^s\right)$ and a new observation ${}^{s_{i:n_s}}\tilde{z}_k = \left\{{}^{s_1}\tilde{z}_k, {}^{s_2}\tilde{z}_k, \cdots {}^{s_{n_s}}\tilde{z}_k\right\}$, where $s_{i:n_s}$ represents the sensor platform that fuses the five statistical texture features simultaneously $(n_s = 5)$. This equation can be derived by using formulas of marginal distribution and conditional independence,

$$p\left(x_k^t \middle| {}^{s_{i:n_s}}\tilde{z}_{1:k}, \tilde{x}_{1:k}^s\right) = \frac{p\left({}^{s_{i:n_s}}\tilde{z}_k \middle| x_k^t, \tilde{x}_k^s\right) p\left(x_k^t \middle| {}^{s_{i:n_s}}\tilde{z}_{1:k-1}, \tilde{x}_{1:k}^s\right)}{p\left({}^{s_{i:n_s}}\tilde{z}_k \middle| {}^{s_{i:n_s}}\tilde{z}_{1:k-1}, \tilde{x}_{1:k}^s\right)} \tag{6}$$

$$p\left({}^{s_{i:n_s}}\tilde{z}_k \middle| {}^{s_{i:n_s}}\tilde{z}_{1:k-1}, \tilde{x}_{1:k}^s\right) = \int p\left({}^{s_{i:n_s}}\tilde{z}_k \middle| x_k^t, \tilde{x}_{1:k}^s\right) p\left(x_k^t \middle| {}^{s_{i:n_s}}\tilde{z}_{1:k-1}, \tilde{x}_{1:k}^s\right) dx_{k-1}^t \tag{7}$$

where $p\left({}^{s_{i:n_s}}\tilde{z}_k \middle| x_k^t, \tilde{x}_{1:k}^s\right)$ refers to the observation likelihood given by the current state, or the sensor model and can be calculated by

$$p\left({}^{s_{i:n_s}}\tilde{z}_k \middle| x_k^t, \tilde{x}_{1:k}^s\right) = \prod_{i=1}^{S_n} p\left({}^{s_i}\tilde{z}_k \middle| x_k^t, \tilde{x}_{1:k}^s\right) \tag{8}$$

Note here that the update at $k = 1$ is implemented by applying $p\left(x_k^t \middle| {}^{s_{i:n_s}}\tilde{z}_{1:k-1}, \tilde{x}_{1:k}^s\right) = p(\tilde{x}_0^t)$.

2) Prediction

The prediction equation computes the probability density function (PDF) of the next step $p\left(x_{k+1}^t \middle| {}^{s_{i:n_s}}\tilde{z}_{1:k}, \tilde{x}_{1:k}^s\right)$ from the PDF in the current step $p\left(x_k^t \middle| {}^{s_{i:n_s}}\tilde{z}_{1:k}, \tilde{x}_{1:k}^s\right)$. This step implemented by Chapman-Kolmogorov equation,

$$p\left(x_{k+1}^t \middle| {}^{s_{i:n_s}}\tilde{z}_{1:k}, \tilde{x}_{1:k}^s\right) = \int p(x_{k+1}^t | x_k^t)\ p\left(x_k^t \middle| {}^{s_{i:n_s}}\tilde{z}_{1:k}, \tilde{x}_{1:k}^s\right) dx_k^t \tag{9}$$

where $p(x_{k+1}^t | x_k^t)$ is a probabilistic Markov motion model that creates a probability map of transition from the current state x_k^t to the next state x_{k+1}^t.

E. Fire heading display

The fire heading estimation computes the vertical horizontal coordinate on the object classified as smoke. This coordinates changes frequently because temperature, air flow, and thermal energy rapidly and unexpectedly changes under fire environments. To cope with this, Kalman filtering is applied to make the vertical and horizontal coordinates of the fire heading stable which leads the robot not to hesitate during navigation.

III. IMPLEMENTATION RESULT

A. Test bed

The experimental test bed consists of a long hallway with two adjacent rooms to describe a general indoor environment as shown in Fig. 5. A 150 mm × 150 mm × 150 mm latex form block and propane gas fires from a 300 mm × 300 mm sand burner were used as fire sources. This sources created dense-low visibility smoke as well as high temperature similar to smoke-filled indoor fire environments. For safety purpose, a remote controlled mobile robot was used instead to collect the perception data in the testing. An A35 thermal camera was installed on the mobile robot at an elevation of 1.75 m which is where SAFFiR camera is also located. The mobile robot was positioned outside of the test bed and started maneuvering when fire and smoke conditions were fully mature in both the hallway and the room. During the experiments, entire thermal images were recorded and analyzed for the fire heading estimation.

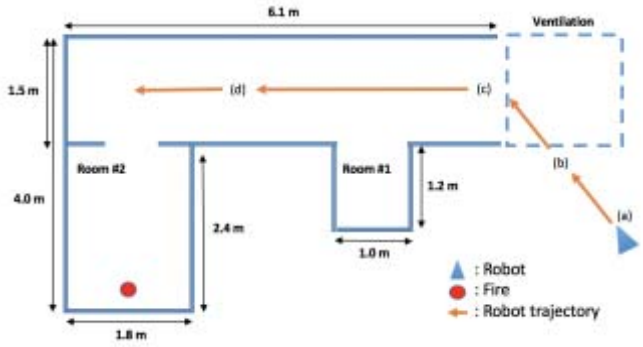

Fig. 5. The experimental test bed where a long hallway and two rooms exist.

B. Results

Figure 6 shows visual, thermal, and probability images with the robot at different locations in the test setup. Fig. 6(a1) contains a RGB image of the robot view at the hallway

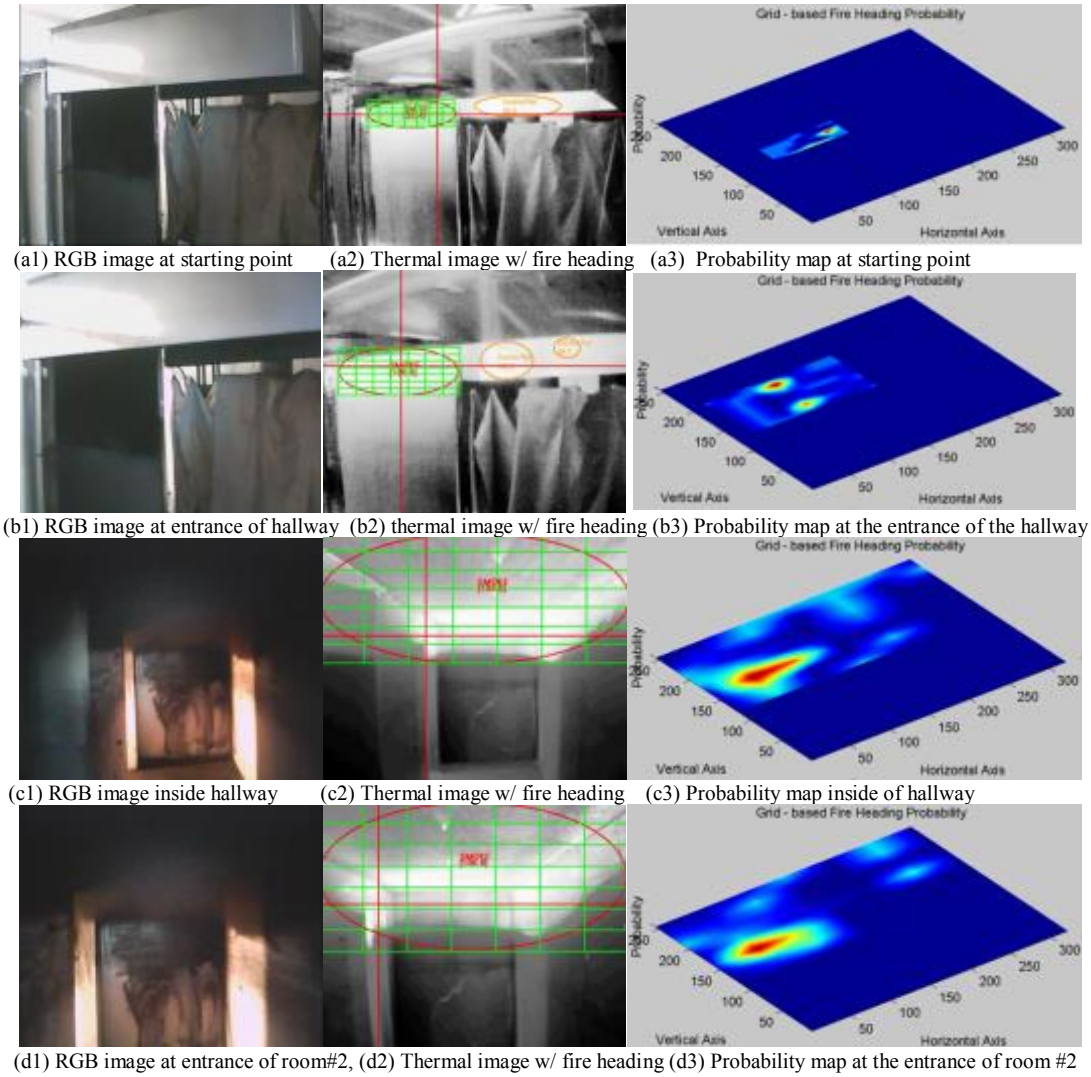

(a1) RGB image at starting point (a2) Thermal image w/ fire heading (a3) Probability map at starting point

(b1) RGB image at entrance of hallway (b2) thermal image w/ fire heading (b3) Probability map at the entrance of the hallway

(c1) RGB image inside hallway (c2) Thermal image w/ fire heading (c3) Probability map inside of hallway

(d1) RGB image at entrance of room#2, (d2) Thermal image w/ fire heading (d3) Probability map at the entrance of room #2

Fig. 6. Results of the fire heading estimation with original RGB images, proceesed thermal images and probability maps at the different location in the test setup.

entrance. As seen in the RGB image, information is not clear due to shadowing of the light. However, as shown in Fig. 6(a2), enhanced thermal image clearly provides classification of smoke and its reflection by displaying their posterior probability on the objects. Also, the fire heading estimation with a red cross over the object classified as smoke indicates where to move. Fig. 6(a3) shows the probability map where the highest is red and the lowest is blue. Fig. 6(b1), (b2) and (b3) show results of the fire heading estimation when the robot moves further toward the hallway entrance. By classifying smoke and its thermal reflections, the fire heading estimates the vertical and horizontal coordinate that leads the robot to navigate toward inside of the test bed where dense smoke is streaming out. Fig. 6(c1) shows an original RGB image of the hallway and Fig. 6(c2) provides the robot with the fire heading direction that precisely indicates the room #2 entrance where the fire exists. Fig. 6(c3) shows that probability at the left and bottom is the highest on the object classified as smoke with 100 % posteriors as shown in the thermal image. Fig. 6(d1), (d2) and (d3) show fire heading results inside the hallway where temperatures are rapidly increasing and hot air flow is suddenly changing as the robot moves further toward the entrance of the room #2. As shown in Fig. 6(d2), the fire heading steadily estimates the direction toward the entrance of room #2 with the red cross.

IV. CONCLUSION

A real-time fire heading estimation in smoke-filled indoor fire environments was presented in order for the firefighting robot to probabilistically identify where to move. The 1st and 2nd order statistical texture features in thermal images were extracted to estimate the highest probability for the heading. Bayesian estimation was used to compute the heading which indicates a horizontal and vertical direction navigating toward the fire outside FOV. For its validation, large-scale fire tests were implemented to create actual fire environments having various ranges of temperature and smoke conditions. Under smoke-filled indoor environments, the fire heading estimates a correct direction on the thermal image with the red cross that indicates the direction toward the room entrance where actual fire occurs.

ACKNOWLEDGMENT

This work was sponsored by the Office of Naval Research Grant No. N00014-11-1-0074. Also, this work has been continuously being researched by National Research Foundation of Korea, Korea Institute of Mechanical & Materials, Wharang-Dae Research Institute.

REFERENCES

[1] J. W. Starr and B. Lattimer, "A comparison of IR stereo vision and LIDAR for use in fire environments," in *Sensors, 2012 IEEE*, 2012, pp. 1-4.

[2] J. W. Starr and B. Lattimer, "Evaluation of Navigation Sensors in Fire Smoke Environments," *Fire Technology,* pp. 1-23, 2012.

[3] J. G. McNeil, J. Starr, and B. Y. Lattimer, "Autonomous Fire Suppression Using Multispectral Sensors," presented at the IEEE/ASME International Conference on Advanced Intelligent Mechatronics (AIM 2013), Wollongong, Austrailia, 2013.

[4] J. W. Starr and B. Y. Lattimer, "Application of Thermal Infrared Stereo Vision in Fire Environments," presented at the IEEE/ASME International Conference on Advanced Intelligent Mechatronics (AIM 2013), Wollongong, Austrailia, 2013.

[5] J.-H. Kim, J. Starr, and B. Lattimer, "Firefighting Robot Stereo Infrared Vision and Radar Sensor Fusion for Imaging through Smoke," *Fire Technology,* pp. 1-23, 2014/06/05 2014.

[6] J.-H. Kim and G. Kim, "Extended Kalman Filter Based Mobile Robot Localization in Indoor Fire Environments," *International Journal of Mechanical Engineering and Robotics Research,* vol. 5, pp. 62-66, 2016.

[7] R. C. Luo and K. L. Su, "Autonomous fire-detection system using adaptive sensory fusion for intelligent security robot," *Mechatronics, IEEE/ASME Transactions on,* vol. 12, pp. 274-281, 2007.

[8] J. A. Milke, M. E. Hulcher, C. L. Worrell, D. T. Gottuk, and F. W. Williams, "Investigation of multi-sensor algorithms for fire detection," *Fire technology,* vol. 39, pp. 363-382, 2003.

[9] H.-C. Kuo and H. Chang, "A real-time shipboard fire-detection system based on grey-fuzzy algorithms," *Fire Safety Journal,* vol. 38, pp. 341-363, 2003.

[10] D. T. Gottuk, S. A. Hill, C. F. Schemel, and B. D. Strehlen, "Identification of fire signatures for shipboard multi-criteria fire detection systems," DTIC Document1999.

[11] F. Amon, V. Benetis, J. Kim, and A. Hamins, "Development of a performance evaluation facility for fire fighting thermal imagers," in *Defense and Security*, 2004, pp. 244-252.

[12] F. Amon, N. Bryner, and A. Hamins, "Evaluation of thermal imaging cameras used in fire fighting applications," in *Defense and Security*, 2004, pp. 44-53.

[13] F. Amon and A. Ducharme, "Image Frequency Analysis for Testing of Fire Service Thermal Imaging Cameras," *Fire technology,* vol. 45, pp. 313-322, 2009.

[14] F. D. Maxwell, "A portable IR system for observing fire thru smoke," *Fire Technology,* vol. 7, pp. 321-331, 1971.

[15] M. I. Chacon-Murguia and F. J. Perez-Vargas, "Thermal video analysis for fire detection using shape regularity and intensity saturation features," in *Pattern Recognition*, ed: Springer, 2011, pp. 118-126.

[16] J.-H. Kim, S. Jo, and B. Y. Lattimer, "Feature Selection for Intelligent Firefighting Robot Classification of Fire, Smoke, and Thermal Reflections Using Thermal Infrared Images," *Journal of Sensors,* 2016.

[17] J.-H. Kim, B. Keller, and B. Y. Lattimer, "Sensor fusion based seek-and-find fire algorithm for intelligent firefighting robot," in *Advanced Intelligent Mechatronics (AIM), 2013 IEEE/ASME International Conference on*, 2013, pp. 1482-1486.

[18] J.-H. Kim and B. Y. Lattimer, "Real-time probabilistic classification of fire and smoke using thermal imagery for intelligent firefighting robot," *Fire Safety Journal,* vol. 72, pp. 40-49, 2015.

[19] O. Barnich and M. Van Droogenbroeck, "ViBe: A universal background subtraction algorithm for video sequences," *Image Processing, IEEE Transactions on,* vol. 20, pp. 1709-1724, 2011.

[20] R. Maini and H. Aggarwal, "Study and comparison of various image edge detection techniques," *International Journal of Image Processing (IJIP),* vol. 3, pp. 1-11, 2009.

[21] N. Otsu, "A threshold selection method from gray-level histograms," *Automatica,* vol. 11, pp. 23-27, 1975.

[22] R. M. Haralick, K. Shanmugam, and I. H. Dinstein, "Textural features for image classification," *Systems, Man and Cybernetics, IEEE Transactions on,* pp. 610-621, 1973.

[23] S. M. Pizer, E. P. Amburn, J. D. Austin, R. Cromartie, A. Geselowitz, T. Greer, *et al.*, "Adaptive histogram equalization and its variations," *Computer vision, graphics, and image processing,* vol. 39, pp. 355-368, 1987.